Energy 96 (2016) 142–154

Contents lists available at ScienceDirect

Energy

journal homepage: www.elsevier.com/locate/energy

Design and preliminary tests of ORC (organic Rankine cycle) with two-stage radial turbine

Seok Hun Kang [a, b, *]

[a] Korea Atomic Energy Research Institute, Daedeok-daero 989-111, Yuseong-gu, Daejeon, 305-353, South Korea
[b] Korea Institute of Energy Research, 152 Gajeong-ro, Yuseong-gu, Daejeon, 305-343, South Korea

ARTICLE INFO

Article history:
Received 24 June 2013
Received in revised form
24 July 2015
Accepted 10 September 2015
Available online 9 January 2016

Keywords:
Organic Rankine cycle (ORC)
Two-stage radial turbine
Low-grade heat
R245fa
Cycle efficiency
Power

ABSTRACT

This paper concerns the design and preliminary tests of the ORC (organic Rankine cycle), which generates electric power using R245fa as a working fluid. A two-stage radial turbine expander is designed with an aim of improving the cycle performance by increasing its pressure ratio. The turbine is coupled with a high-speed generator without gear box incurring speed reduction. The turbine is designed in consideration of the thermodynamic properties of the working fluid and the cycle conditions. The design processes of the turbine and cycle are presented in the paper. The performance of the developed cycle and the turbine is examined experimentally, and the factors which influence the performance of the developed ORC are analyzed.

1. Introduction

Rapidly increasing fossil fuel consumption has led to many serious energy and environmental problems such as global warming, air pollution, and depletion of the ozone layer, as well as energy shortages and security issues. As a result, many researches are focusing on the utilization of low-grade heat sources. The ORC (organic Rankine cycle) is regarded as one of the most suitable methods of converting low-grade heat into power among several well-known technologies including the supercritical Rankine cycle, the Kalina cycle, and the trilateral flash cycle [1–3]. The ORC is also known to have superior characteristics in terms of its simplicity and availability, and is already widely applied in many practical areas [4].

The ORC has the same system configuration as the steam Rankine cycle, but it uses organic fluids with low boiling points as a working fluid. The main merit of the ORC is that it is able to generate power using low temperature heat sources like industrial exhausting heat, geothermal heat, and solar thermal energy because of the low boiling point and high evaporation pressure properties of its working fluid. In addition, the ORC is characterized by its simple structure, high reliability, and ease of maintenance [1]. The expander of the ORC is more compact than that of the steam Rankine cycle, since the density of the ORC's working fluid is higher than that of steam. Furthermore, the compactness and efficiency of the ORC can be enhanced by utilizing a dry working fluid as it does not need a super-heater [5]. A considerable amount of research is being conducted on its application for the energy recovery from industrial exhausting heat, biomass energy, the internal combustion engines of ships and cars, solar and geothermal energies, etc.

The ORC technology was demonstrated back in the late seventies and early eighties [6–8]. Today, ORC systems for large-scale industrial heat recovery, biomass and geothermal plants are commercially produced by just a few companies (TRUBODEN, ORMAT, Barber-Nichols, etc.) possessing strong turbine design and manufacturing technologies [9–11]. However, many researches are still being performed with the aim of developing a small-scale (kW scale) system and the technology required for its application to internal combustion engines of cars or ships, solar and geothermal energies, and micro CHP (combined heat and power) systems [8].

A large body of numerical and experimental research has been conducted concerning the ORC, and a number of experimental works have risen remarkably from a decade ago. However, most of the results of thermal efficiency tests conducted in previous studies were found to be low, which was mainly due to the small capacities

* Korea Atomic Energy Research Institute, Daedeok-daero 989-111, Yuseong-gu, Daejeon, 305-353, South Korea. Tel.: +82 42 868 8080; fax: +82 42 868 2075.
E-mail addresses: shkang73@gmail.com, kang@kaeri.re.kr.

http://dx.doi.org/10.1016/j.energy.2015.09.040
0360-5442/

(lower than 10 kW) of the proposed systems. In addition, only a few researches have been conducted on the development of a high-efficiency expander machine whose design took into consideration the system's characteristics such as the cycle operation conditions and the thermodynamic properties of the working fluid. In most of the previous researches, the ORC expanders were designed by utilizing the existing screw, scroll and turbine compressors in the reverse mode, which were themselves modified from commercial refrigeration systems [3,8,12].

Bao et al. presented a comprehensive review of the working fluid selection and the choice of expansion machines for use in the ORC system [1]. They analyzed the influence of the working fluids' types and thermophysical properties on the ORC's performance, as well as the design and operating characteristics of various expansion machines such as turbine, screw, scroll and piston expanders. Recently published experimental researches are as follows. Bracco et al. designed a prototype ORC, and showed the test results obtained in stationary and transient operating conditions. A small-sized (about 1 kWe) scroll expander and a generator from the compressor component of an existing commercial HVAC (heating, ventilation and air conditioning) were installed in the system [13]. Declaye et al. investigated the experimental characteristics of an open-drive scroll expander integrated into an ORC using R245fa as the working fluid. The expander was a commercial air compressor modified to operate in the expander mode. A maximum cycle efficiency of 8.5% was investigated [8]. Aleksandra presented experimental investigations of the hermetic turbogenerator installed in the ORC plant operating with R227ea as the working fluid, and the ORC's electric efficiency was observed to be 4.88% [12]. Li et al. experimentally analyzed the effect of varying the working fluid mass flow rate and the regenerator on the efficiency of an ORC operating on R123. A single-stage axial flow turbine was installed in the system, and a generator was connected to the turbine with a coupler. The experimental results of the power output and the ORC efficiency were shown to be 6.07 kW and 7.98% [3]. Qiu et al. presented an experimental investigation involving a biomass-fired ORC, for which a vane-type air compressor was modified and used as an expander. The electricity generation efficiency and power output were observed to be 1.41% and 861 kW [14]. Lee et al. examined the transient responses of a 50 kW ORC subject to change of the water coolant in the condenser with R245fa as the working fluid, and presented the effect of varying the water coolant flow rate in the condenser on the system's performance [4]. Pei et al. constructed a 3.75 kW ORC system using an R123, and applied a radial turbine to the ORC; the result of their experiment showed isentropic turbine efficiency of 62.5%, while the ORC efficiencies based on turbine shaft power and electricity output were 6.6% and 3.0%, respectively [10]. Quoiline et al. presented both a numerical model of an ORC and an experimental study of a prototype working with an R123. A scroll expander was used, and its isentropic effectiveness ranged from 42% to 68%. The maximum cycle efficiency was 7.4%. The pressure ratio over the expander varied from 2.7 to 5.4, and its influence on the system performance was observed [15]. Wang et al. developed a prototype ORC with a cooling capacity of 5 kW and tested it under laboratory conditions. They applied micro-channel-based heat transfer components and a scroll-based expander to the ORC. The measured isentropic efficiency of the scroll expander reached 84% [16]. Nguyen et al. developed a prototype ORC using n-pentane as the working fluid. A radial turbine coupled to a high-speed alternator directly was used. The power output, thermal efficiency and isentropic turbine efficiency were found to be 1.47 kW, 4.3% and 49.8%, respectively, when the evaporator-condenser pressure ratio was 4.07 [17]. Manolakos et al. presented the on-site experimental evaluation of the performance of a low-temperature solar ORC. Solar heat and HFC-134a were used as the heat source and working fluid, respectively [18]. Kane et al. designed and tested a small hybrid solar power system composed of an ORC comprising a hermetic scroll expander-generator and solar collectors [19]. Yun et al. proposed and evaluated ORC with multi expanders in parallel and experimentally evaluated the feasibility and the fundamental characteristics of the proposed ORC by testing it in different operating modes [20]. Peris et al. characterized the system performance of the ORC designed and built for CHP application and the expander performance through test for micro-CHP applications [21,22]. They also verified the performance of ORC operating in actual industrial conditions and assessed its profitability [23]. Cho et al. conducted experimental study to develop the ORC utilizing fluctuating thermal energy source [24]. Fu et al. designed a 250 kW ORC using turbine expander, and presented the preliminary results under off-design conditions [25]. Jung et al. demonstrated the feasibility of using a zeotropic mixture as working fluid through an experimental study with a 1 kW ORC unit [26]. Lecompte ea al. presented an overview of ORC architectures and the available experimental data [27]. Hu et al. conducted a detailed design and off-design performance analysis based on the preliminary design of turbines and heat exchangers, and presented performance data [28]. Minea investigated the technical feasibility of 50 kW prototype ORC using industrial waste or renewable energy sources at temperatures varying between 85 °C and 116 °C [29]. Xing et al. investigated condensation heat transfer of R245fa in a tube and the effect of inclination angle [30]. Higashi et al. presented R245fa properties measured with two types of isochoric methods [31]. Song et al. reviewed the application and research status of the scroll expander applied to ORC, including its technical features, performances and the main technical limitations existing in application [32].

An expander is a key component that affects the efficiency, size and cost of the ORC system. Generally, expanders are categorized as two types: the velocity type, such as turbine expanders, and the volume type, such as screw, scroll and piston expanders [1,13]. The turbine expander is recognized for its high efficiency and compactness, compared to volume type ones. But it has disadvantages such as high cost and low efficiency in off-design conditions [1]. The turbo expander is categorized as axial and radial types. The axial turbine has a superior advantage in the high expansion ratio which can be increased by adding the expansion stage [9,10]. On the other hand, the radial turbine is known to be suitable for system conditions where the flow rate is low, and is more compact than the axial one [33,34].

Cycle performance is significantly influenced not only by turbine efficiency but also by its expansion ratio. The increases in the turbine expansion ratio and the evaporator-condenser pressure ratio result in improvements in the Carnot and cycle efficiencies. However, the radial turbine, which typically has a single-stage, is limited in terms of increasing the expansion ratio. Generally, the expansion ratio of a single-stage radial turbine is known to be about 4 [34], but such a small value restricts the increase of the pressure ratio [35].

From this perspective, a two-stage radial turbine composed of a HPT (high-pressure turbine) and a LPT (low-pressure turbine) is designed to increase the expansion ratio and to compensate for the weak points of the single-stage one. An ORC capable of producing 40 kW of electric power is also designed. R245fa is adopted as the working fluid, as it is suitable for cycle operation conditions, and is environmentally friendly and safe [16,36]. The R245fa has been used in many studies because of its thermodynamic suitability for low-temperature heat recovery and environmentally friendly and safe characteristics, and its molecular weight, critical pressure and

critical temperature are 134 g/mol, 3640 kPa and 427.2 K, respectively [30,31,33,37,38]. Preliminary tests are conducted to investigate the performance characteristics of the designed ORC with a two-stage radial turbine. Finally, some cautions regarding the design or selection of the pump are mentioned with a view to improving the system's reliability. To the writer's knowledge, no experimental research on an ORC using a two-stage radial turbine has been published as yet.

2. Cycle layout and design

Fig. 1 shows the schematic diagram of the designed ORC system. Its main components are the turbine, evaporator, condenser, storage tank and pump. The steam and water circuits are represented by dashed lines, signifying the heat source and coolant. The flow direction arrows for the working fluid, heat source and coolant under normal operating conditions are shown as well as the measurement positions for temperature, pressure and flow rate. The liquid state working fluid in the storage tank is pressurized, and supplied to the evaporator by the pump. Then, the working fluid is vaporized in the evaporator, which is heated by a heat source supplied via the boiler. The vapor state working fluid flows into the turbine, where it expands and produces power. The superheated vapor at the turbine outlet is condensed through the condenser, which is cooled by a coolant from the cooling tower cooled by outdoor air. Then, the condensed working fluid flows into the storage tank. Figs. 2 and 3 show a drawing and a photograph of the constructed ORC.

The thermodynamic cycle design process, which is similar to that of the former process [39], is briefly described as follows. The condensation temperature and pressure are considered as the basis of this cycle design. The atmo $\eta_{t,is} = \frac{h_{HPT,i} - h_{LPT,o}}{h_{HPT,i} - h_{LPT,o,is}}$ spheric air is used as a heat sink, whose temperature is assumed to be 20 °C in the design procedure. The condensation temperature is set to 10 °C higher than the heat sink temperature, and the condensation pressure is set to a saturation value, i.e. 1.78 bar, of working fluid at that temperature. The evaporation temperature is designed to be 120 °C considering the pressure ratio of the turbine, the capacity of the heat exchanger and the allowable pressure limit of the system. The evaporation pressure is also set to the saturation value, i.e., 19.3 bar. Thus, the pressure ratio between the evaporator and the condenser is 10.8 (19.3/1.78), which is used in the turbine design as an expansion ratio between its inlet and outlet.

Considering the high pressure ratio of the cycle, a two-stage radial turbine, rather than a single-stage one, composed of an HPT and an LPT, is designed (It will be explained in greater detail in the next section). Thus, the working fluid expands in the HPT and LPT sequentially. The isentropic turbine efficiency is assumed to be 80% for the prediction of turbine outlet conditions in the design procedure, and is defined by Equation (1) [3,10,35].

$$\eta_{t,is} = \frac{h_{HPT,i} - h_{LPT,o}}{h_{HPT,i} - h_{LPT,o,is}} \tag{1}$$

where $\eta_{t,is}$ is the isentropic turbine efficiency, $h_{HTP,i}$ is the specific enthalpy of the working fluid at the turbine inlet, i.e., HPT inlet, $h_{LPT,o,is}$ is the specific enthalpy of the working fluid at the turbine outlet, i.e., the LPT outlet, when its entropy is the same as that at the turbine inlet. $h_{LPT,o}$ is the specific enthalpy of the working fluid at the turbine outlet, and is determined from this equation.

Table 1 shows the thermodynamic properties of the working fluid at each cycle design point. Fig. 4 shows temperature versus entropy (T-s) diagram of the designed cycle. The thermodynamic properties are calculated using REFPROPP 8.0 [40].

The working fluid flow rate is set to 1.5 kg/s in consideration of the capacities of the system components including the turbine, evaporator, condenser and pump, and is designed to be determined according to the turbine nozzle throat area at the designed expansion ratio (10.8).

Then the turbine shaft power defined by Equation (2) is calculated as 52.5 kW.

$$\dot{W}_{sh} = \dot{m}\ \left(h_{HPT,i} - h_{LPT,o}\right) \tag{2}$$

where $\dot{m}$ is the mass flow rate, and $\dot{W}_{sh}$ is the shaft power of the turbine.

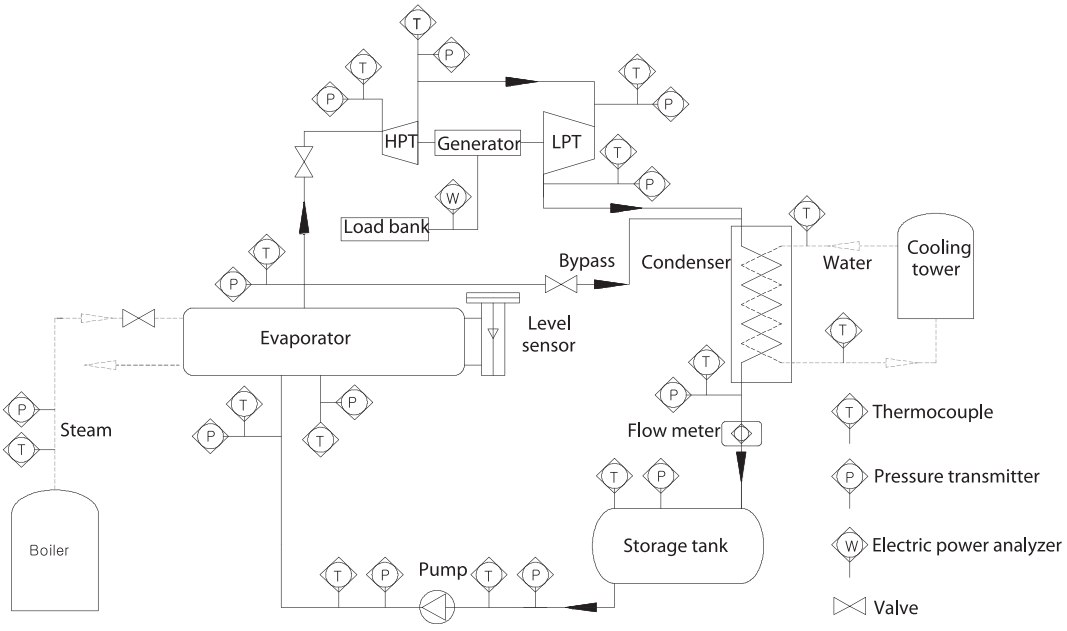

Fig. 1. Schematic diagram of the designed ORC system.

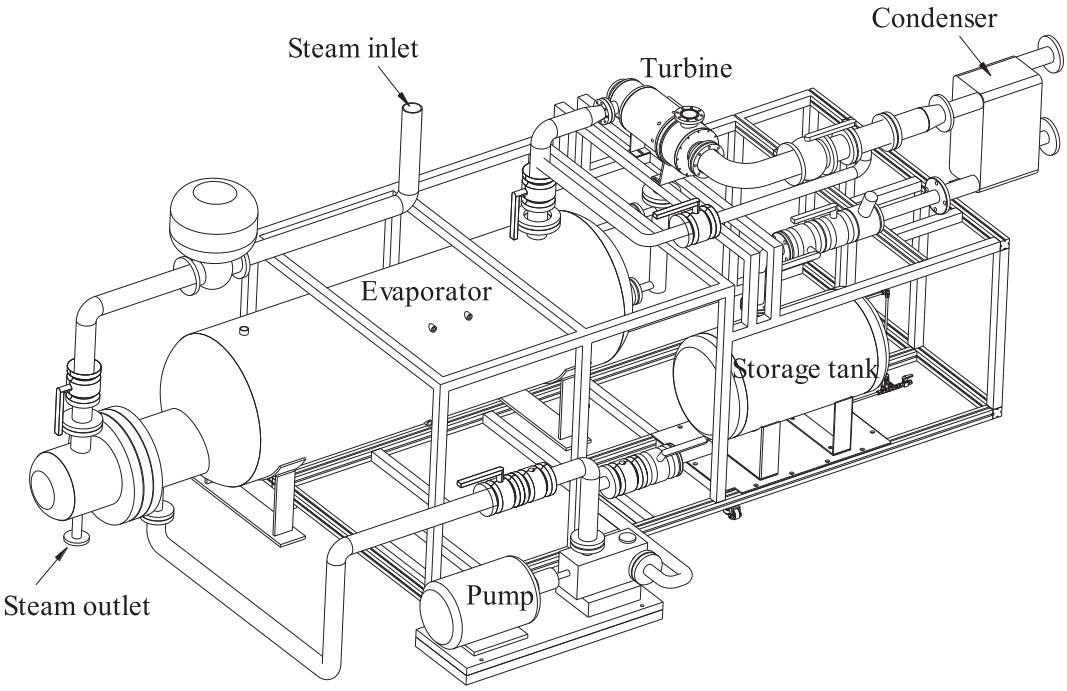

Fig. 2. Drawing of ORC system.

Fig. 3. Photograph of developed system.

The electrical and mechanical loss in the generator is assumed to be 20% in the turbine design procedure, and the turbine output based on electricity is calculated as 42 kW using Equation (3).

$$\dot{W}_t = \varepsilon \dot{W}_{sh} \tag{3}$$

where $\dot{W}_t$ is the power output of the turbine measured by a power meter, and ε is the electrical and mechanical loss factor in the generator.

The cycle efficiency is calculated as 11.2% using Equation (4) below, ignoring the pressure and heat losses incurred in the entire system [35].

$$\eta_{th} = \frac{\dot{W}_t - \dot{W}_p}{\dot{m} \cdot (h_{e,o} - h_{p,o})} \tag{4}$$

where η_{th} is the cycle efficiency, $h_{e,o}$ is the specific enthalpy of the working fluid at the evaporator outlet, $h_{p,o}$ is the specific enthalpy

Table 1
Thermodynamic properties of working fluid at cycle design points.

Design points	Temperature (°C)	Pressure (bar)	Enthalpy (kJ/kg)	Entropy (kJ/kg-K)	Density (kg/m^3)
(a) Saturated liquid at pump inlet	30	1.78	239	1.14	1325
(b) Compressed liquid at pump outlet	30	1.93	240	1.13	1331
(c) Saturated liquid in evaporator	120	19.3	373	1.51	999
(d) Saturated vapor in evaporator	120	19.3	484	1.80	120
(e) Superheated vapor at turbine outlet	54	1.78	449	1.83	9.22
(f) Saturated vapor in condenser	30	1.78	426	1.75	10.2

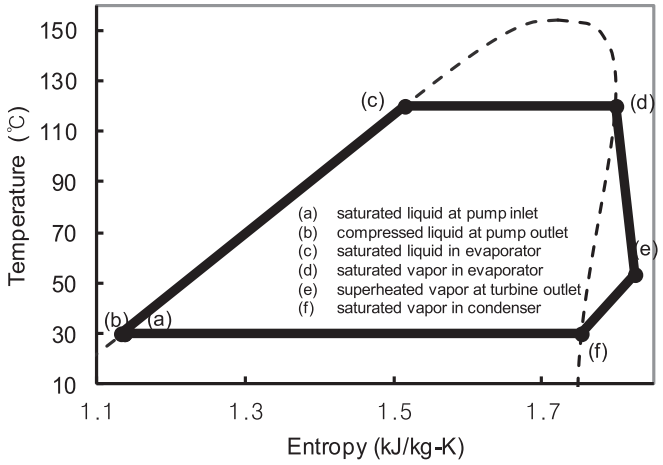

Fig. 4. T-s diagram of the designed cycle.

of the working fluid at the pump outlet. $\dot{W}_p$ is the power consumed by the pump, and is calculated using Equation (5) as follows:

$$\dot{W}_p = \dot{m} \cdot (h_{p,o} - h_{p,i}) \tag{5}$$

where $h_{p,i}$ is the specific enthalpy of the working fluid at the pump inlet. The power consumption of the pump is generally negligible compared with the power output of the turbine [35].

The evaporator pressure is to be the saturation value, and is determined by the evaporation temperature. Thus a shell-and-tube type heat exchanger is selected as the evaporator, as it contains working fluid in both liquid and vapor states to produce saturated vapor. The evaporation temperature is to be controlled by adjusting the flow rate of the heat source which is 150 °C saturated steam produced from the gas-fired boiler. The level of the liquid state working fluid in the evaporator is to be controlled by a float-type level sensor and a pump. Fig. 5 is a schematic drawing of the evaporator whose heat exchange capacity is set at 440 kW, which has a margin of about 20% compared with the amount of heat exchange calculated by Equation (6) at the design points.

$$C_e = \dot{m} \ (h_{e,o} - h_{p,o}) \tag{6}$$

where C_e is the amount of heat exchange of the evaporator.

The compact brazed-type heat exchanger is used for the condenser considering the compactness of the system. The condensation pressure is to be a saturation value by connecting the condenser outlet to the storage tank containing the liquid state working fluid. The heat exchange capacity of the condenser is set at 380 kW, having a margin of about 20% compared with the amount of heat exchange calculated by Equation (7) at the design points.

$$C_c = \dot{m} \ (h_{c,i} - h_{c,o}) \tag{7}$$

where C_c is the heat exchange capacity of the condenser, $h_{c,i}$ is the specific enthalpy of the working fluid at the condenser inlet, and $h_{c,o}$ is the specific enthalpy of the working fluid at the condenser outlet.

A screw-type pump is used as it offers an advantage over the impeller type in that it prevents cavitation. The pump is connected with an inverter, and its rotational speed is to be adjusted by converting the frequency to control the flow rate using a working fluid level signal from the evaporator with PID logic.

The evaporator is designed and manufactured by Sungsan Ltd; the condenser is supplied by Sungsan Ltd (model WP10L-190 from GEA GmbH); the storage tank designed in a cylindrical shape with a volume of 200 L is manufactured by MEPS Ltd; the pipe and control systems are manufactured by MEPS Ltd; and the circulation pump is supplied by Jinsol Ltd (model IMO3 - screw pump).

3. Turbine design

A radial type turbine is adopted as the expander for the designed ORC, after considering its high performance characteristics under

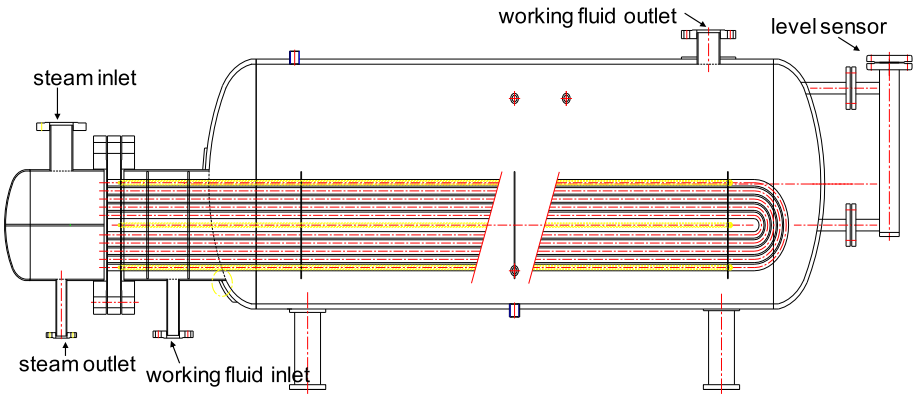

Fig. 5. Schematic drawing of evaporator.

small capacity and flow rate conditions. In addition, the radial turbine has the merit of compactness when it is in operation with a high-density working fluid.

It is decided that the turbine should consist of two-stage expansion processes through the HPT and LPT in consideration of the high pressure ratio of the system, as explained in the previous section. Figs. 6 and 7 show a photograph and drawings of the proposed turbine.

The preliminary design of the turbine is made in order to calculate the needed size, angle and number of blades and nozzles by considering the thermodynamic properties of the working fluid and the cycle operation condition. However, it is difficult to design both an optimal LPT and HPT for this study, largely because the two turbines are designed to be connected in the same shaft, and to rotate at the same number of revolutions despite the differences in their design parameters. Thus the efficiency of the LPT is considered to be more important than that of the HPT in the design procedure, considering the low pressure at its outlet which is connected to the condenser. The expansion ratio of the LPT is designed to be 4.07, while that of the HPT is to be determined depending upon that of the LPT. Additionally, the rotational speed of the HPT is fixed to that of the LPT value, which is designed to be 21,200 rpm. The number of nozzle vanes installed on the LPT and the HPT is set at 20. The results of the preliminary turbine design are shown in Table 2.

The efficiency of the radial turbine can be estimated by taking into account the specific speed and specific diameter in the design procedure. The maximum efficiency is known to be about 90% [34]. However, this estimation does not consider the size effect. Thus the results of the typical gas dynamic design incorporating the experimental correlations show that the estimated turbine efficiency is about 85%. Moreover, most radial turbine design theory deals with ideal gas, while the working fluid used in this research is not a thermally perfect gas. Therefore, it is expected that the existing turbine design software can lead to a certain degree of uncertainty in the design of a turbine using organic fluid. Instead, a three-dimensional turbine blade is designed based on the geometrical similarity of the existing model turbine and the results of the preliminary design. Table 3 shows the design specifications of the model turbine, while Figs. 8 and 9 show drawings and photographs of the developed turbine blade and nozzle. The LPT and HPT rotor blades are designed to be located at the end of the shaft as shown in Fig. 7. The blades and nozzles are made of aluminum because of the ease with which it can be processed and because of its lightness.

A brushless synchronous-type generator employing a permanent magnet rotor is used for its high rotational speed, i.e., 21,200 rpm, under normal operational conditions, and its compactness in terms of mechanical configuration, weight and size. The rotor of the generator is designed to be located on the middle of the turbine shaft, and is shown in Fig. 10. Grease-packed ball bearings are used to support the shaft of the rotor.

The electrical capacity of the generator is designed to be 42 kW at the nominal rotational speed of 21,200 rpm. The generator is designed to be connected to the rotor blades directly, and to run with the rotational speed of the turbine shaft, without any speed reduction resulting from the use of a gear box. Fig. 11 shows a photograph of the manufactured stator of the generator. Silicon steel plates, which are suitable for high-frequency generators, are used in the stator of the generator, using the plates having a thickness of 0.2 mm. The SmCo permanent magnet is used as the material of the rotor of the generator. The generated power is designed to be dissipated through the load bank, and to be measured by a power analyzer.

Long-term operation tests for the proposed turbine have not been conducted. Its reliability may be limited due to the use of ball bearings (See Fig. 7(b)) that require lubrication, and of the aluminum material that is weak in terms of its durability. The utilization of air foil bearings that do not need lubrication and high-strength materials may increase the reliability of the turbine.

4. Experiment description

Preliminary experimental tests are conducted to assess the performance of the designed ORC and the turbine under a range of conditions. While operating the system, the thermodynamic properties of the working fluid in the cycle are calculated by REFROPP 8.0 [40] using measured temperature and pressure values. Sensors for measuring the temperature, pressure, flow rate and electric power are installed in the cycle, as shown in Fig. 1.

The working fluid is circulated through the by-pass line instead of driving the turbine in the start-up stage prior to heating up the entire system. Then, the experimental data are measured for 4 evaporation temperature steps, which are set at 113, 114, 115 and 116 °C in the control panel, to investigate the performance of the developed system near its design conditions. The average outdoor air temperature is 4 °C during the experiment, which is much lower than the design value (20 °C). A steady state is maintained for about 20 min to gather data in each evaporation temperature step. The evaporation temperature is controlled by adjusting the flow rate of the heat source through PID logic on the basis of the temperature of the working fluid at the evaporator outlet. On the other hand, the condensation temperature is not controlled as the cooling water flow rate is

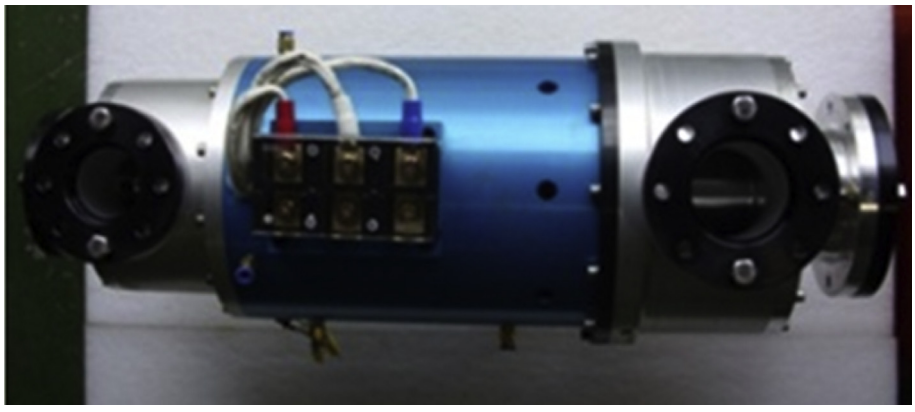

Fig. 6. Photograph of manufactured turbine.

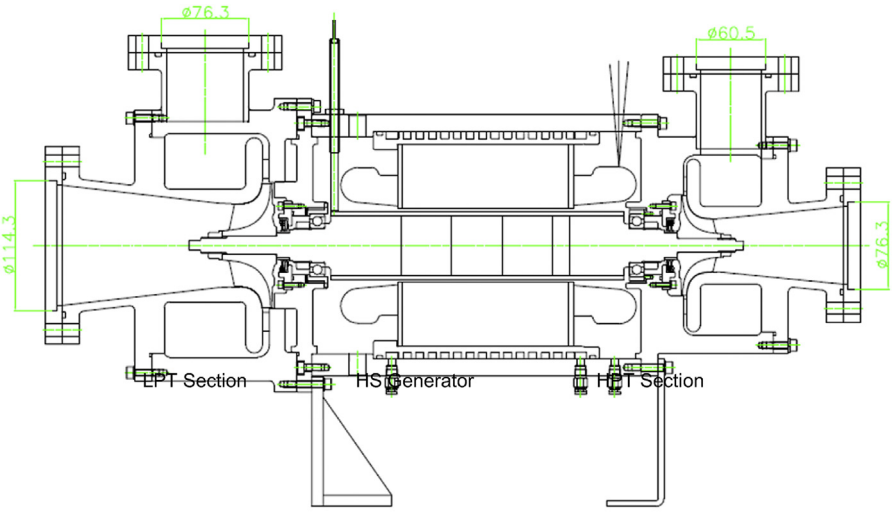

(a) Mechanical configuration

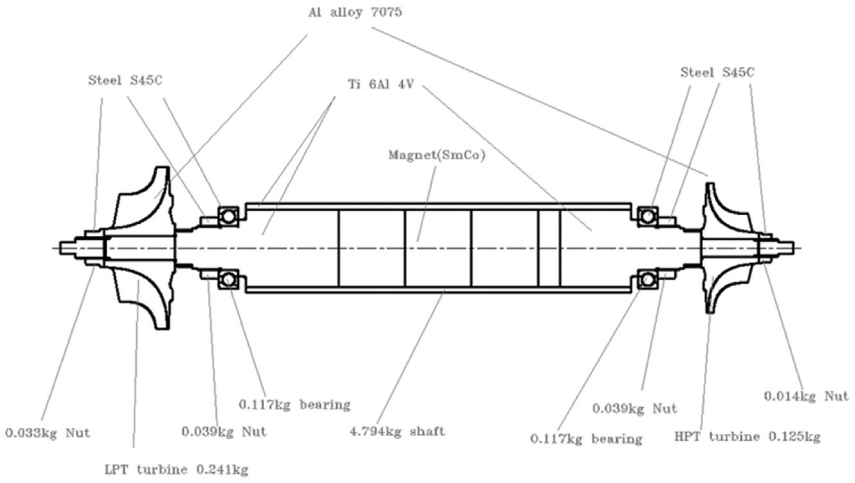

(b) Schematic drawing of blades, rotor and its supports

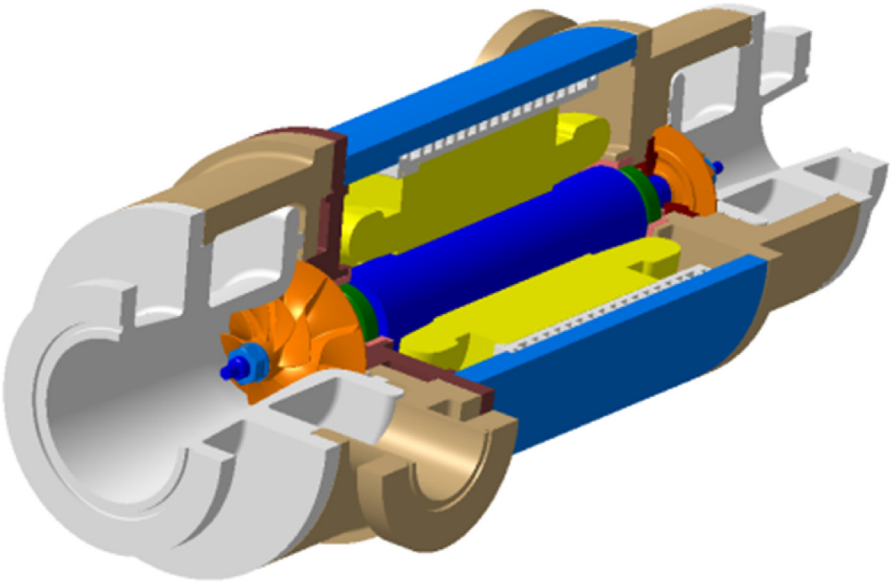

(c) 3-D drawing

Fig. 7. Drawings of turbogenerator.

Table 2
Preliminary turbine design data.

Parameters		Unit	Values
Mass flow rate		kg/s	1.58
Power		kW	42
Rotational velocity		rpm	21,200
Isentropic efficiency		%	80
HPT	Inlet temperature	°C	120
	Inlet pressure	bar	19.3
	Exit temperature	°C	89.3
	Exit pressure	bar	7.48
	Rotor inlet tip radius	mm	43.7
	Rotor exit rip radius	mm	29.1
	Rotor exit hub radius	mm	10.7
	Nozzle throat area	mm^2	321.5
	Nozzle exit velocity	m/s	114.8
	Nozzle number	ea	20
	Nozzle inlet angle to radial direction	degree	0
	Blade inlet angle to radial direction	degree	0
	Nozzle exit angle to radial direction	degree	75.9
	Blade exit angle to radial direction	degree	58.8
LPT	Inlet temperature	°C	88.7
	Inlet pressure	bar	7.24
	Exit temperature	°C	54
	Exit pressure	bar	1.78
	Rotor inlet tip radius	mm	54.4
	Rotor exit rip radius	mm	36.3
	Rotor exit hub radius	mm	13.3
	Nozzle throat area	mm^2	494.6
	Nozzle exit velocity	m/s	140.0
	Nozzle number	ea	20
	Nozzle inlet angle to radial direction	degree	0
	Blade inlet angle to radial direction	degree	0
	Nozzle exit angle to radial direction	degree	75.9
	Blade exit angle to radial direction	degree	58.8

Table 3
Design specifications of model turbine (working fluid is air).

Parameters	Unit	Value
Power capacity	kW	190
Rotational speed	rpm	63,000
Mass flow rate	kg/s	0.6
Expansion ratio		3.6
Isentropic efficiency	%	84
Nozzle inlet radius	mm	124
Nozzle vane height	mm	10
Nozzle throat area	mm^2	1366
Rotor inlet radius	mm	90
Rotor exit radius at tip	mm	60
Rotor exit radius at hub	mm	22

maintained at its full capacity, which is 18 kg/s, regardless of the cycle operation condition.

All temperatures and pressures are measured with type-T thermocouples with an accuracy of ±0.5 °C (made by SSK) and pressure transducers made by Valcom with accuracy of ±0.25% over the full scale range (2.0 Mpa). The working fluid flow rate is measured using a turbine-type flow meter made by Blancett (model B111-110/B-2500) with a rate of accuracy of ±0.5%. The electric power output of the generator is measured using a power analyzer made by Yokogawa (model WT3000), with a rate of accuracy of ±0.02%. All the measurement data are recorded and stored on a computer by using the NI CompactDAQ, a data acquisition system. The uncertainty in the measurement is calculated using the root-sum-square method [16,41]. The percentage uncertainties of the turbine and the cycle efficiencies are found to be lower than 2.24% and 2.34%.

The system has stopped frequently during its operation due to corrosion of the rotating parts of the pump, but cavitation has not taken place. The corrosion features of the pump parts to the working fluid should be considered when selecting or designing the pump.

5. Results

Figs. 12–18 show the experimental results over time. Table 4 shows the average values of thermodynamic properties obtained at key measurement positions for evaporation temperatures. Table 5 lists the average results of the power, efficiencies, expansion ratio, and mass flow rate with evaporation temperatures.

Fig. 12 shows the variations in the evaporation and condensation temperatures and pressures over time. The evaporation temperature increases from about 113 to 116 °C, and the evaporation pressure increased proportionally to it from 17.4 to 18.6 bar. While the condensation temperature and pressure remain almost constant, with their average values of 18.3 °C and 1.42 bar, respectively. The condensation temperature results are lower than the design value (30 °C). The reason for this is the low outdoor temperature (4 °C) compared to its design value (20 °C). This causes the evaporation temperature not to rise to its design value (120 °C) since the heat exchange capacity of the evaporator is not sufficient to increase the evaporation temperature to the design value (120 °C) from such a low condensation temperature.

Fig. 14 shows the variations in temperature and pressure at the turbine inlet and outlet over time. The HPT inlet temperature increases from about 113 to 116 °C, and the HPT inlet pressure increases proportionally to it, varying from about 17.2 to 18.4 bar. While the variations in temperature and pressure at the HPT outlet and the LPT inlet are shown to be almost marginal. The average temperatures of the HPT outlet and the LPT inlet are 83.3 and 82.9 °C, and their average pressures are 6.38 and 5.87 bar, respectively. The differences in temperature and pressure between the

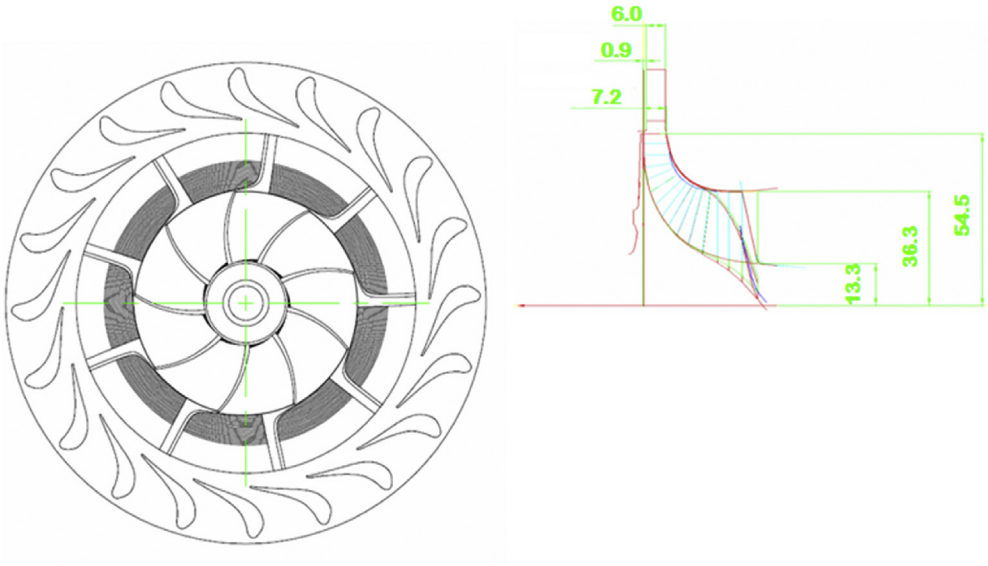

Fig. 8. Drawings of LPT rotor and nozzle.

Fig. 9. Photographs of turbine nozzles and rotors.

HPT outlet and the LPT inlet seem to be caused by thermal and friction losses of the working fluid flow in the pipe connecting the HPT outlet with the LPT inlet, leading to deterioration in the turbine performance. The average LPT outlet pressure is 1.62 bar, which is also higher than the average condensation pressure (1.42 bar, see Fig. 13). This difference appears to be the result of a pressure drop in the condensation heat exchanger. This pressure loss reduces the efficiency of the cycle and the turbine, decreasing the pressure ratio between the turbine inlet and the outlet.

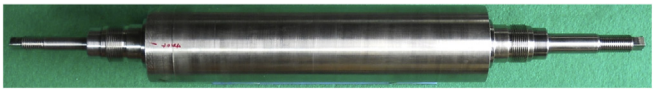

Fig. 10. Photograph of generator rotor.

Fig. 15 shows the expansion ratios of the entire turbine, HPT and LPT over time. The expansion ratio of the turbine is the pressure ratio between the HPT inlet and the LPT outlet in Fig. 15. And the expansion ratios of the HPT and LPT are the pressure ratios between their inlet and outlet. The turbine expansion ratio increases over

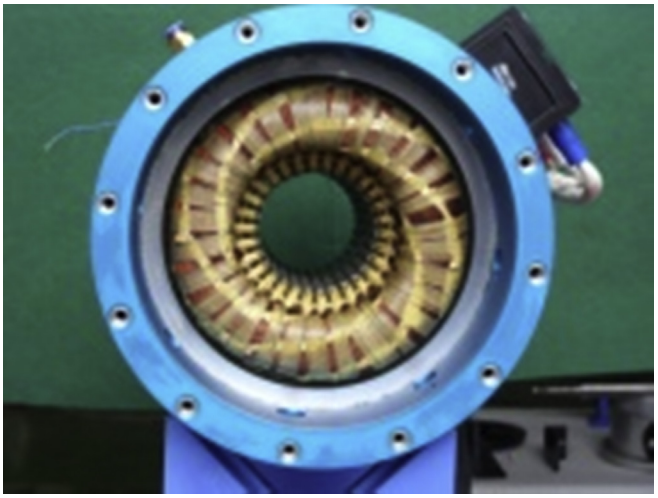

Fig. 11. Photograph of generator stator.

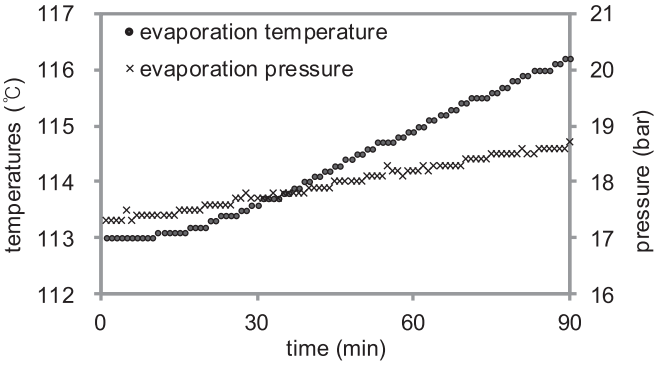

Fig. 12. Evaporation temperature and pressure with time.

time in accordance with the rise in the evaporation pressure elevation, as shown in Fig. 12, with the average values ranging from 10.9 to 11.6, as in Table 5. The expansion ratio results are found to be slightly higher than the design value (10.8). This is mainly thought to be due to the lower condensation pressure results compared to the design value. The expansion ratio of the LPT is found to be larger than that of HPT, as predicted in the design procedure.

Fig. 16 shows the power output and the mass flow rate of the working fluid over time. The power output increases from about 33 to 39 kW as the evaporation pressure, see Fig. 12, and the mass flow rate increases over time.

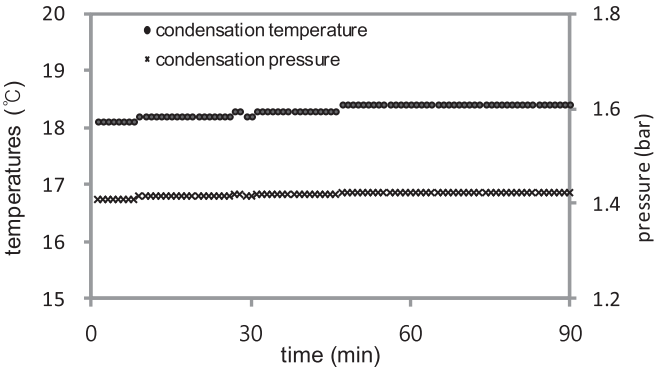

Fig. 13. Condensation temperature and pressure with time.

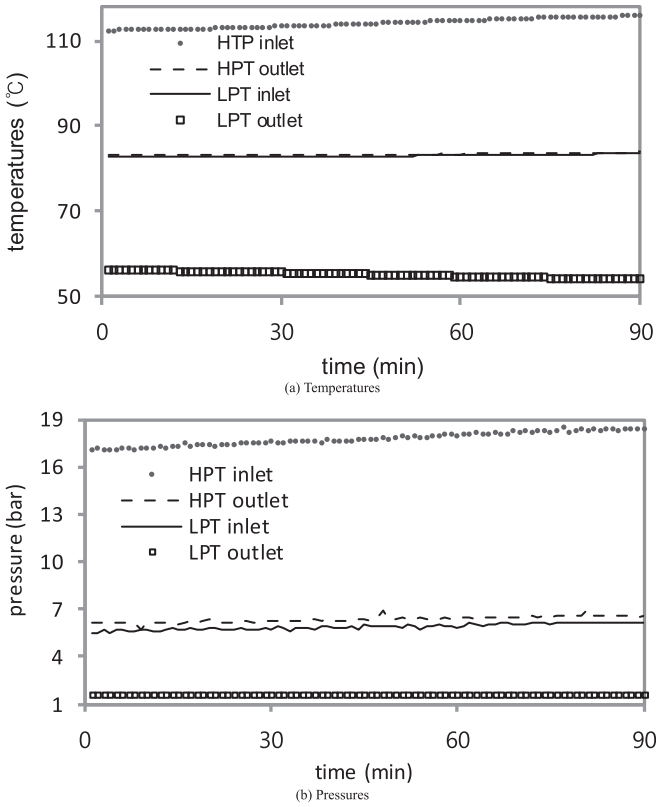

Fig. 14. Variation of turbine temperatures and pressures with time.

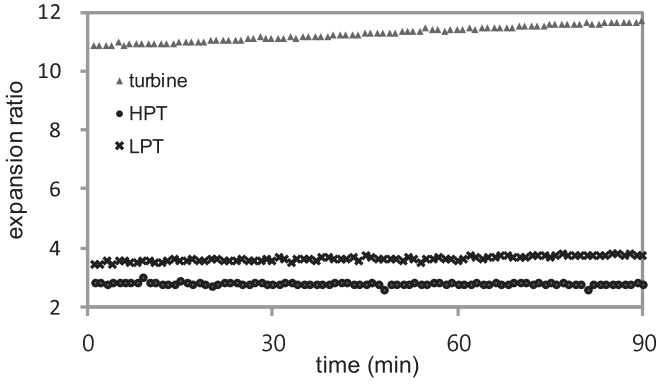

Fig. 15. Expansion ratios with time.

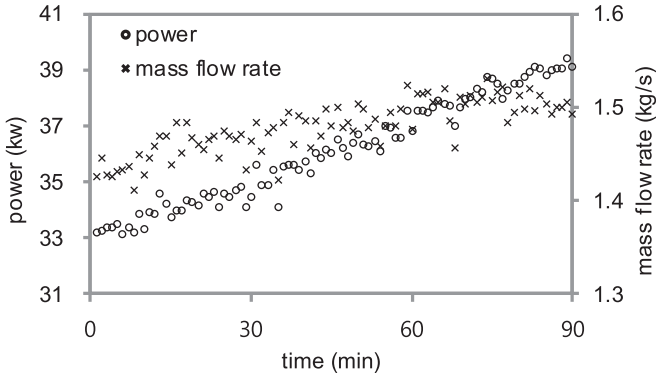

Fig. 16. Power output and mass flow rate with time.

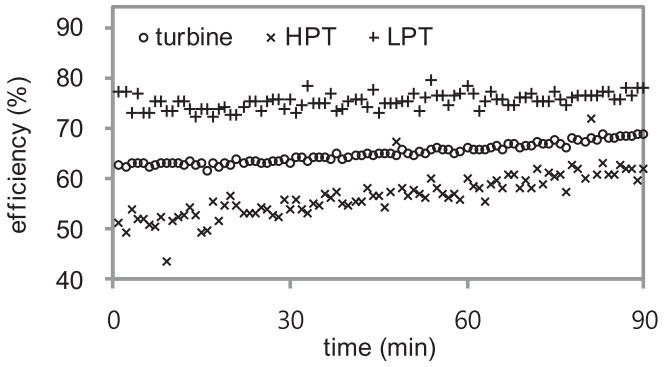

Fig. 17. Isentropic turbine efficiencies with time.

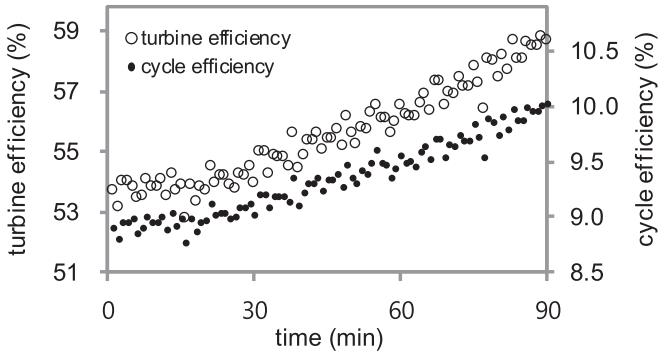

Fig. 18. Cycle and turbine efficiencies with time.

Fig. 17 shows the isentropic efficiencies of the turbine, HPT and LPT; they are calculated using Equations (1), (8a) and (8b).

$$\eta_{HPT,is} = \frac{h_{t,i} - h_{HPT,o}}{h_{t,i} - h_{HPT,o,is}} \tag{8a}$$

$$\eta_{LPT,is} = \frac{h_{LPT,i} - h_{LPT,o}}{h_{LPT,i} - h_{LPT,o,is1}} \tag{8b}$$

where $\eta_{HPT,is}$ and $\eta_{LPT,is}$ represent the isentropic efficiencies of the HPT and LPT, respectively, $h_{HTP,o}$ is the specific enthalpy of the working fluid at the HPT outlet, $h_{HTP,o,is}$ is the specific enthalpy of the working fluid at the HTP outlet when its entropy is the same as that at the HTP inlet, $h_{LPT,i}$ is the specific enthalpy of the working fluid at the LPT inlet, and $h_{LPT,o,is1}$ is the specific enthalpy of the working fluid at the LPT outlet when its entropy is the same as that at the LPT inlet. The isentropic efficiency of the LPT is higher than that of the HPT as is intended in the design procedure. This is thought to be due to the fact that the efficiency of the LPT is more highly considered than that of the HPT in design procedure as explained in section 3, and the expansion performance of LPT is superior to that of HPT as shown in Fig. 15.

Fig. 18 shows the cycle and turbine efficiencies based on the electric power output over time. They are obtained from Equations (4) and (9), respectively.

$$\eta_t = \frac{\dot{W}_t}{\dot{m}\ (h_{HPT,i} - h_{LPT,o,is})} \tag{9}$$

where η_t is the turbine efficiency. The cycle and turbine efficiencies shown in Fig. 18 increase over time. The increase of turbine efficiency seems to be caused by the increases of expansion ratio and enthalpy difference at the turbine inlet and outlet over time. The increase of cycle efficiency is thought to be caused by the increases of power output and turbine efficiency over time.

The average maximum power, turbine and cycle efficiencies based on the power output are found to be 39.0 kW, 58.4% and 9.8% when the evaporation temperature is 116 °C as seen in Table 5. The results of previous experiments with small-scale ORC comprising single-stage turbines are listed in Table 6 for a comparison with this work [3,10,17,39]. The turbine efficiency results obtained in this study are lower than that of author's previous study [39]. This seems to be due to the fact that the turbine proposed in this study is

Table 4
Experimental results of thermodynamic properties of working fluid.

Evaporator		Position	Temperature (°C)	Pressure (Bar)	Enthalpy (kJ/kg)	Entropy (kJ/kg-K)
Temperature (°C)	Pressure (Bar)					
113	17.4	Pump inlet	18.1	1.41	223	1.08
		Pump outlet	18.1	17.4	224	1.08
		Evaporator	113	17.4	361	1.48
		HTP inlet	113	17.2	479	1.79
		LPT inlet	82.6	5.62	470	1.82
		LTP outlet	56.0	1.60	452	1.84
114	17.9	Pump inlet	18.3	1.42	224	1.08
		Pump outlet	18.3	17.9	224	1.08
		Evaporator inlet	114	17.9	362	1.49
		HTP inlet	114	17.8	479	1.79
		LPT inlet	82.8	5.85	470	1.82
		LTP outlet	55.2	1.60	451	1.84
115	18.3	Pump inlet	18.4	1.42	224	1.08
		Pump outlet	18.4	18.3	224	1.08
		Evaporator inlet	115	18.3	364	1.49
		HTP inlet	115	18.1	479	1.79
		LPT inlet	83.0	6.00	470	1.82
		LTP outlet	54.6	1.60	451	1.84
116	18.6	Pump inlet	18.4	1.42	224	1.08
		Pump outlet	18.4	18.6	224	1.08
		Evaporator inlet	116	18.6	366	1.50
		HTP inlet	116	18.4	480	1.79
		LPT inlet	83.4	6.15	470	1.82
		LTP outlet	54.0	1.60	450	1.83

Table 5
Average experimental results for evaporation temperatures.

Evaporation temperature (°C)	Power (kW)	Isentropic turbine efficiency (%)			Turbine efficiency based on power output (%)	Cycle efficiency (%)	Expansion ratio	Mass flow rate kg/s
		Whole turbine	HPT	LPT				
113	33.4	63.1	44.8	74.9	53.7	8.91	10.9	1.43
114	35.6	64.1	47.1	74.5	54.7	9.16	11.2	1.49
115	37.6	65.9	49.5	75.1	56.2	9.44	11.4	1.52
116	39.0	68.5	52.1	76.5	58.4	9.80	11.6	1.52

Table 6
List of experimental work on the small-scale ORC with radial turbine.

Researchers	Working fluid	Turbine type	Turbine efficiency (%)	Cycle efficiency (%)	Power (kW)	Evaporator-condenser pressure ratio
Nguyen et al. [17]	n-pentane	single-stage radial	49.8 (isentropic)	4.3	1.47	4.07
Kang [39]	R245fa	single-stage radial	78.7 (based on power)	5.22	32.7	2.72
Pei et al. [10]	R123	single-stage radial	62.5 (isentropic)	3.0	3.75	4.29
Li et al. [3]	R123	single-stage axial	58.5 (isentropic)	7.98	6.07	5.14

not optimally designed as explained in section 3. On the other hand, the cycle efficiency results obtained in the present study in Table 6 are shown to be superior to the results of previous studies in Table 7 [39] despite the reduction in turbine efficiency. This is thought to be largely attributable to the high evaporator-condenser pressure ratios which are found to be at least two times higher than those of previous studies, and to the adoption of a two-stage turbine with a high expansion ratio capability.

The developed system has not yet been operated in its exact design condition. This is mainly due to such factors as the low outdoor air temperature, which affects the condensation temperature; losses in the system; and difficulties in controlling the main components. Furthermore, the performance of the turbine, which largely affects the cycle operation conditions such as the working fluid flow rate and power, cannot be predicted with great precision in the design procedure, and the turbine cannot be operated in its design conditions.

6. Conclusion

In this study, design and experimental procedures are carried out with the aim of investigating the performance of an ORC with a two-stage radial turbine. The design procedures for the cycle and the turbine as well as the related experimental results are presented. The turbine is designed to be composed of two-stage expansion processes to increase expansion ratio, and is coupled with a high-speed generator producing electric power.

The performance and operational characteristics of the developed system are examined by conducting preliminary tests. The maximum electric power, average cycle and turbine efficiencies based on power output are found to be 39.0 kW, 9.8% and 58.4%, respectively. An improvement of cycle performance relative to the findings of similar previous researches results is observed, and this improvement is thought to be due to the increases observed in the evaporator-condenser pressure and turbine expansion ratios.

Further work is required to improve the ORC's performance, such as reducing the heat and pressure losses in the entire system and increasing the performance of the main components including the turbine, generator, and heat exchangers.

Acknowledgment

This work was supported by the National Research Foundation of Korea (NRF) grant funded by the Korean government (MSIP: Ministry of Science, ICT and Future Planning) (No. 2011-0031933) and KIER (Korea Institute of Energy Research).

References

[1] Bao J, Zhao L. A review of working fluid and expander selections for organic Rankine cycle. Renew Sustain Energy Rev 2013;24:325–42.
[2] Chen H, Goswami DY, Stefanakos EK. A review of thermodynamic cycles and working fluids for the conversion of low-grade heat. Renew Sustain Energy Rev 2010;14:3059–67.
[3] Li M, Wang J, He W, Lin Gao, Wang B, Ma S, et al. Construction and preliminary test of a low-temperature regenerative organic Rankine cycle (ORC) using R123. Renew Energy 2013;57:216–22.
[4] Lee YR, Kuo CR, Wang CC. Transient response of a 50 kW organic Rankine cycle system. Energy 2012;48:532–8.
[5] Aljundi Isam H. Effect of dry hydrocarbons and critical point temperature on the efficiencies of organic Rankine cycle. Renew Energy 2011;36:1196–202.
[6] Casci C, Angelino G, Ferrari P, Gaia M, Giglioli G, Macchi E. Experimental results and economics of a small (40 kW) organic Rankine engine. In: Int. 15th intersociety energy conversion engineering conference, Seattle, Washington; August 1980. p. 1008–14.
[7] McKenna RF. Organic Rankine cycle silent power plant, 1.5 kW, 28VDC. Report for electrotechnology department, electromechanial division. U.S. Army Mobility R&D Center; 1975. http://www.ntis.gov/search/product.aspx?abbr%bcADA000900.
[8] Declaye S, Quoilin S. Experimental study on an open-drive scroll expander integrated into an ORC (Organic Rankine Cycle) system with R245fa as working fluid. Energy 2013;55:173–83.
[9] Quoilin S, Broek M, et al. Techno-economic survey of organic Rankine cycle (ORC) system. Renew Sustain Energy Rev 2013;22:168–86.
[10] Pei G, Li J, Li Y, Wang D, Ji J. Construction and dynamic test of a small-scale organic Rankine cycle. Energy 2011;36:3215–23.
[11] Lai NA, Wendland M, Fischer J. Working fluids for high-temperature organic Rankine cycles. Energy 2011;36:199–211.
[12] Aleksandra BG. Experimental investigation of R227ea applied as working fluid in the ORC power plant with hermetic turbogenerator. Appl Therm Eng 2013;56:126–33.
[13] Bracco R, Clemente S, Micheli D, Reini M. Experimental tests and modelization of a domestic-scale ORC (Organic Rankine Cycle). Energy 2013;58:107–16.
[14] Qiu G, Shao Y, Li J, Liu H, Riffat SB. Experimental investigation of a biomass-fired ORC-based micro-CHP for domestic applications. Fuel 2012;96:374–82.
[15] Quoilin S, Lemort V, Lebrun J. Experimental study and modelling of an organic Rankine cycle using scroll expander. Appl Energy 2010;87:1260–8.
[16] Wang H, Peterson R, Harada K, Miller E, Ingram R, Fisher L. Performance of a combined organic Rankine cycle and vapor compression cycle for heat activated cooling. Energy 2011;36(1):447–58.
[17] Nguyen V, Doherty P, Riffat S. Development of a prototype low-temperature Rankine cycle electricity generation system. Appl Therm Eng 2001;21:169–81.
[18] Manolakos D, Kosmadakis G, Kyritsis S, Papadakis G. On site experimental evaluation of a low-temperature solar organic Rankine cycle system for RO desalination. Sol Energy 2009;83:646–56.
[19] Kane M, Larrain D, Favrat D, Allani Y. Small hybrid solar power system. Energy 2003;28:1427–43.
[20] Yun E, Kim D, Yoon SY, Kim KC. Experimental investigation of an organic Rankine cycle with multiple expanders used in parallel. Appl Energy 2015;145:246–54.
[21] Peris B, Navarro-Esbri J, Moles F, Gonzalez M. Experimental characterization of an ORC (organic Rankine cycle) for power and CHP (combined heat and power) applications from low grade heat source. Energy 2015;82:269–76.
[22] Peris B, Navarro-Esbri J, Moles F, Marti JP, Mota-Babiloni A. Experimental characterization of an organic Rankine cycle (ORC) for micro-scale CHP applications 2015;79:1–8.

[23] Peris B, Navarro-Esbri N, Moles F, Mota-Babiloni A. Experimental study of an ORC (organic Rankine cycle) for low grade waste heat recovery in a ceramic industry. Energy 2015;85:534–42.
[24] Cho SY, Cho CH. An experimental study on the organic Rankine cycle to determine as to how efficiently utilize fluctuating thermal energy. Renew Energy 2015;80:73–9.
[25] Fu BR, Lee YR, Hsieh JC. Design, construction, and preliminary results of a 250-kW organic Rankine cycle system. Appl Therm Eng 2015:80339–46.
[26] Jung HC, Taylor L, Krumdieck S. An experimental and modelling study of a 1 kW organic Rankine cycle unit with mixture working fluid. Energy 2015;81:601–14.
[27] Lecompte S, Huisseune H, Broek M, Vanslambrouck B, Paepe MD. Review of organic Rankine cycle (ORC) architectures for waste heat recovery. Renew Sustain Energy Rev 2015;47:448–61.
[28] Hu D, Li S, Zheng Y, Wang J, Dai Y. Preliminary design and off-design performance analysis of an organic Rankine cycle for geothermal sources. Energy Convers Manag 2015;96:175–87.
[29] Minea V. Power generation with ORC machines using low-grade waste heat or renewable energy. Appl Therm Eng 2014;69:143–54.
[30] Xing F, Xu J, Xie J, Liu H, Wang Z, Ma X. Froude number dominates condensation heat transfer of R245fa in tubes: effect of inclination angles. Int J Multiph Flow 2015;71:98–115.
[31] Higashi Y, Hayasaka S, Shirai C, Akasaka R. Measurements of PrT properties, vapor pressures, saturated densities, and critical parameters for R 1234ze(Z) and R 245fa. Int J Refrig 2015;52:100–8.
[32] Song P. A review of scroll expanders for organic Rankine cycle systems. Appl Therm Eng 2015;75:54–64.
[33] Rahbar K, Mahmoud S, Al-Dadah RK, Moazami N. Parametric analysis and optimization of a small-scale radial turbine for organic Rankine Cycle. Energy 2015;83:696–711.
[34] Balje OE. Turbomachines: a guide to design selection and theory. New York: John Wiley & Sons; 1981.
[35] Wylen G, Sonntag R, Borgnakke C. Fundamentals of classical thermodynamics. 4th ed. John Wiley & Sons, Inc; 1993.
[36] Larjola J. Electricity from industrial waste heat using high-speed organic Rankine cycle (ORC). Int J Prod Econ 1995;41:227–35.
[37] Wang EH, Zhang HG, Fan BY, Ouyang MG, Zhao Y, Mu QH. Study of working fluid selection of organic Rankine cycle (ORC) for engine waste heat recovery. Energy 2011;36:3406–18.
[38] Wang XD, Zhao L, Wang JL, Zhang WZ, Zhao XZ, Wu W. Performance evaluation of a low-temperature solar Rankine cycle system utilizing R245fa. Sol Energy 2010;84:353–64.
[39] Kang SH. Design and experimental study of ORC (organic Rankine cycle) and radial turbine using R245fa working fluid. Energy 2012;41:514–24.
[40] Lemmon E, Huber M, McLinden M. NIST REFPROP standard reference database 23. Version 8.0 user's guide. 2007.
[41] Figliola R, Beasley D. Theory and design for mechanical measurements. 3rd ed. John Wiley & Sons, Inc; 1995.